Carbon 115 (2017) 503–514

Contents lists available at ScienceDirect

Carbon

journal homepage: www.elsevier.com/locate/carbon

Poly(vinylidene fluoride) derived fluorine-doped magnetic carbon nanoadsorbents for enhanced chromium removal

Yonghai Cao [a, b, 1], Jiangnan Huang [a, b, 1], Xiangfang Peng [a, *], Dapeng Cao [c, **], Alexandra Galaska [a], Song Qiu [d], Jiurong Liu [d], Mojammel A. Khan [e], David P. Young [e], Jong Eun Ryu [f], Hongbo Feng [g], Narendranath Yerra [h], Zhanhu Guo [b, ***]

[a] Laboratory of Polymer Processing Engineering of Ministry of Education, South China University of Technology, Guangzhou, Guangdong 510640, PR China
[b] Integrated Composites Laboratory (ICL), Department of Chemical and Biomolecular Engineering, University of Tennessee, Knoxville, TN 37996, United States
[c] State Key Lab of Organic-Inorganic Composites, Beijing University of Chemical Technology, Beijing, 100029, PR China
[d] School of Materials Science and Engineering, Shandong University, Jinan, Shandong, 250061, PR China
[e] Department of Physics and Astronomy, Louisiana State University, Baton Rouge, LA 70803, United States
[f] Department of Mechanical Engineering, Indiana University - Purdue University Indianapolis, IN 46202, United States
[g] Department of Chemistry, University of Tennessee, Knoxville, TN 37996, United States
[h] Engineered Multifunctional Composites (EMC) Nanotech LLC, Knoxville, TN 37934, United States

ARTICLE INFO

Article history:
Received 4 November 2016
Received in revised form
11 January 2017
Accepted 12 January 2017
Available online 13 January 2017

ABSTRACT

Newly designed fluorine-doped magnetic carbon (F-MC) was synthesized in situ though a facile one-step pyrolysis-carbonization method. Poly(vinylidene fluoride) (PVDF) served as the precursor for both carbon and fluorine. 2.5% F content with core-shell structure was obtained over F-MC, which was used as a adsorbent for the Cr(VI) removal. To our best knowledge, this is the first time to report that the fluorine doped material was applied for the Cr(VI) removal, demonstrating very high removal capacity (1423.4 mg g^{-1}), higher than most reported adsorbents. The unexpected performance of F-MC can be attributed to the configuration of F dopants on the surface. The observed pseudo-second-order kinetic study indicated the dominance of chemical adsorption for this process. High stability of F-MC after 5 recycling test for the Cr(VI) removal was also observed, indicating that F-MC could be used as an excellent adsorbent for the toxic heavy metal removal from the wastewater.

1. Introduction

The effective disposal of wastewater for the heavy metal removal is attracting more and more attention in the social and academic communities. Cr(VI), a classical heavy metal pollutant emitted from the industrialization, is one of the most toxic metal ions in the surface water [1]. Trace amount of Cr(VI) will cause serious physiological and neurological damages. As reported that the concentration range of Cr(VI) ions in wastewater was about 60–1800 mg/L [2,3]. Be aware of this problem, less than 100 μg L^{-1} of the total Cr in drinking water is permitted to protect the human body [4]. Thus, it is indispensable to remove Cr(VI) from waste water for further utilization. In order to improve the removal efficiency, various methods have been developed, such as ion exchange, chemical precipitation, membrane separation, biosorption and reverse osmosis [5–9]. Among those technologies, adsorption is considered as the most suitable method for the industries due to its high efficiency, low cost and independence on facilities without any side-products and second-pollution. Several adsorbents, i.e., bio-absorbents, clay minerals, metal phosphates, zeolites, active carbon and magnetic carbons, have been utilized in the environmental remediation [10–17]. Recently, magnetic carbons have recently drawn a great deal of interests due to their highly porous structure with easy-controllable chemical properties and the magnetization for the separation [1,15,16,18–20]. For example, Qiu et al. recently synthesized the magnetic carbons by one-step pyrolysis of cellulose and $Fe(NO_3)_3$ with high activity for the Cr(VI)

* Corresponding author.
** Corresponding author.
*** Corresponding author.
E-mail addresses: pmxfpeng@scut.edu.cn (X. Peng), caodp@mail.buct.edu.cn (D. Cao), zguo10@utk.edu (Z. Guo).
[1] These authors contributed equally.

http://dx.doi.org/10.1016/j.carbon.2017.01.033
0008-6223/

removal (maximum capacity (q_{max}) is 327.5 mg g^{-1}, pH = 2) [1]. In this process, the redox reaction between the Cr(VI) ions and magnetic nanoparticles (Fe) played a significant role for the Cr(VI) removal. After treatment, the magnetic carbon showed a good magnetism and could be easily separated. Nevertheless, these magnetic adsorbents displayed a relatively low efficiency for the Cr(VI) removal.

Recently, surface modification with heteroatoms, such as nitrogen, sulfur et al., is a new approach for enhancing the ability of environmental remediation [21–25]. For instance, Qiu and co-workers found that the polyethylenimine (PEI) facilitated ethyl cellulose and fibers displayed an excellent performance for Cr(VI) removal in a wide pH range. After modified by PEI, the adsorption capacity (36.8 mg g^{-1}) was greatly enhanced, higher than the unmodified sample (12 mg g^{-1}) [21]. The doping of heteroatoms, such as nitrogen and sulfur et al., into the adsorbents is another approach for enhanced environmental remediation [24–26]. The heteroatoms can adjust the negative charge density on the surface of adsorbent, therefore facilitating the adsorption of contaminants [24,25,27,28]. For example, Shin and co-workers reported that nitrogen doped magnetic carbon nanoparticles (N-MCs), fabricated by the pyrrole and ferric chloride, displayed a good performance in the adsorption of heavy metal. The adsorption on the surface of N-MCs took place through a chemical process involving the valence forces. The enhanced adsorption capacity of heavy metal ions over nitrogen doped sample was 10 folds higher than the undoped active carbon [29]. Nitrogen doping greatly enhanced the removal efficiency of carbon due to the improved interaction between the adsorbents and Cr(VI) ions [30]. More recently, fluorination was proposed as a novel process for the surface modification to improve the performance [31–35]. Many efforts were made to prepare the fluorine modified anatase materials to reduce the Cr(VI) to Cr(III) ions in the photocatalysis. For instance, Song and his co-workers synthesized fluorinated TiO_2 nanostructures for the Cr(VI) removal and obtained a rate constant 7 times greater than that achieved using pure-TiO_2. The surface fluorination facilitates the adsorption process by increasing the number of surface OH groups generated, thus enhancing the adsorption ability [33]. These results indicated that the fluorination was a promising approach to clean waste water. For the carbon materials, the fluorine atoms can increase electron transfer as well as high electronegative fluorine functionalities [32]. Nevertheless, in the case of environmental remediation, there has been very little research reported on the waste water treatment by the fluorine doped carbon adsorbents.

In this work, fluorine doped magnetic carbons (F-MC) were synthesized through a simple one-step thermal pyrolysis method using poly(vinylidene fluoride) (PVDF) as carbon and fluorine precursor. To our best knowledge, it is the first time to report the Cr(VI) ions removal by fluorine doped adsorbent with considerable activity and stability. The influence of Cr(VI) concentration, adsorbents loading, adsorption time, pH and the adsorption kinetics were investigated in detail. The complex relationships between the physical/chemical properties of adsorbent and Cr(VI) removal efficiency were correlated to reveal the enhancement of F dopant for the Cr(VI) removal.

2. Experimental section

2.1. Materials

Potassium dichromate (99%, $K_2Cr_2O_7$), 1,5-diphenylcarbazide (97%, DPC) and ethanol (99%) were purchased from Alfa Aesar Company. $Fe(NO_3)_3{\cdot}9H_2O$ (99%), sodium hydroxide (NaOH, 99.1%), sulfuric acid (H_2SO_4, 95%), phosphoric acid (H_3PO_4, 85%), PVDF (99%) and glucose (99%) were obtained from Fisher Scientific Ltd. All the chemicals were used as received without any further purification.

2.2. Synthesis of F-MCs nanoadsorbents

The F-MCs were synthesized as follows. Typically, 6 g $Fe(NO_3)_3{\cdot}9H_2O$ and 3 g PVDF were added into ethyl alcohol solvent (100 mL) and then treated under ultra-sonication for 2 h to be mixed intensively. After that, the mixture was dried at 110 °C overnight. The obtained solid samples then were carbonized at 800 °C for 2 h under N_2 atmosphere. To control the fluorine doped levels, glucose was added into mixtures to adjust the PVDF concentration at 0, 33, 50, 66 and 100 wt%, which were noted as the F-MC-0, F-MC-33, F-MC-50, F-MC-66 and F-MC-100, respectively.

2.3. Characterization

Transmission electron microscope (TEM) images were obtained with a FEI Tecnai G2 12 microscope operated at 100 kV. The samples were prepared by ultrasonically suspending in acetone and depositing several drops of the suspension onto a grid. Scanning electron microscope (SEM) images were obtained with a FEI Quanta 600F electron microscope. X-ray diffraction (XRD) patterns were obtained from a Bruker D8 ADVANCE diffractometer equipped with a rotating anode using Cu Kα radiation (40 kV, 40 mA). Raman spectra were obtained in a LabRAM Aramis micro Raman spectrometer with an excitation wavelength at 532 nm with 2 mm spot size. X-ray photoelectron spectroscopy (XPS) were performed in a Kratos Axis ultra (DLD) spectrometer equipped with an Al Kα X-ray source in ultrahigh vacuum (UHV) ($<10^{-10}$ Torr). The binding energies were referenced to the C_{1s} peak at 284.6 eV. Brunauer-Emmett-Teller (BET) specific surface areas were measured by N_2 adsorption at liquid N_2 temperature in an ASAP 2010 analyzer. The magnetic property measurements were carried out in a 2 T physical property measurement system (PPMS) by Quantum Design at room temperature.

2.4. The removal of Cr(VI)

Typically, the selected nanoadsorbents were added into the Cr(VI) solution and treated under ultrasonication for certain time at room temperature. Cr(VI) removal efficiency based on the effects of different Cr(VI) concentration, treatment time and pH value (measured by a pH meter, Vernier Lab Quest with pH-BTA sensor) were investigated in detail. The Cr(VI) concentration in solution was measured by the colorimetric method[7] by using the obtained standard fitting Equation (1):

$$C_e = 3.8716A\text{-}0.00039 \quad (1)$$

where C_e is the concentration of Cr(VI) and A is the absorbance at 540 nm obtained from the UV–vis test.

The Cr(VI) removal percentage (R%) was calculated using Equation (2):

$$R\% = \frac{(C_0 - C_e)}{C_0} \times 100\% \quad (2)$$

where C_0 and C_e (mg L^{-1}) are the Cr(VI) concentrations in solution before and after treatment, respectively. The removal capacity (q_e, mg g^{-1}) is quantified by Equation (3):

$$q_e = \frac{(C_0 - C_e)V}{m} \times 100\% \quad (3)$$

where V (L) represents the volume of Cr(VI) solution and m (g) is the mass of the used magnetic carbon nanoadsorbents.

3. Results and discussion

3.1. Synthesis of F-MCs

Fig. 1 shows the typical SEM and TEM images of as-synthesized samples. All of the samples displayed nanospheres with core-shell structure. From Fig. 1a, the MC displayed the core-shell structure with a carbon coating at about 3–5 nm. With the addition of PVDF (Fig. 1b–e, g to j), much more amorphous carbons were synthesized, and the particles were covered by the amorphous carbons. The sizes of particles in F-MCs were random. Meanwhile, the thickness of carbon coating increased with the increasing of PVDF loading from 33 wt% to 100 wt%. The tightly interconnected nanospheres by the amorphous carbons were also observed in the F-MCs, benefiting the synthesis of zero valence iron (ZVI, the redox reaction between carbon and FeO_x) [1]. The XRD pattern evidenced that four kinds of iron state existed on the surface of all the samples (Fig. 2). Large amount of ZVI particles were observed, indicating that the FeO_x were partially reduced by the PVDF or glucose during the calcination process [36]. In addition, iron (II) fluoride (FeF_2) nanoparticles were observed after adding the PVDF with even a small amount (33 wt%) into the precursor, attributing to the synthetic reaction between the PVDF and $Fe(NO_3)_3$ during the carbonization process, i.e., $CF_x + FeO_x \rightarrow CO_2 + FeF_2$ [36–38]. With increasing the addition of PVDF, the FeF_2 became dominant in the adsorbents, which was also observed in the porous Fe_3O_4-FeF_2@CFx composites for the electrochemistry [36–38].

These fluorine functionalities in this work endowed stronger adsorption ability for the metal ions [23–25,29]. Therefore, the fluorine content of doped magnetic carbons was measured by XPS (Figs. 3 and S1, Table 1). The full-range XPS survey demonstrated four main peaks such as C_{1s}, O_{1s}, F_{1s} and Fe_{2p}, located at about 284.6, 530, 685 and 711 eV, respectively, indicating that F atoms were successfully incorporated into the magnetic carbons during the carbonization procedure. From Table 1, alone with the increase of PVDF loading, the atomic ratio in the F-MCs increased from 0% to 2.5%. The F1s spectra of doped magnetic carbons were then deconvoluted into four peaks centered at about 684.8, 685.8, 687.3 and 689.2 eV, which could be assigned to FeF_2 (F1), ionic C-F (F2), semi-ionic C-F (F3) and covalent C-F (F4), respectively [36,39–41]. A large portion of FeF_2 with 31%–45% was observed over F-MCs, confirming the previous discussion in the XRD section [36]. In addition, abundance of ionic C-F bond and semi-ionic C-F bond

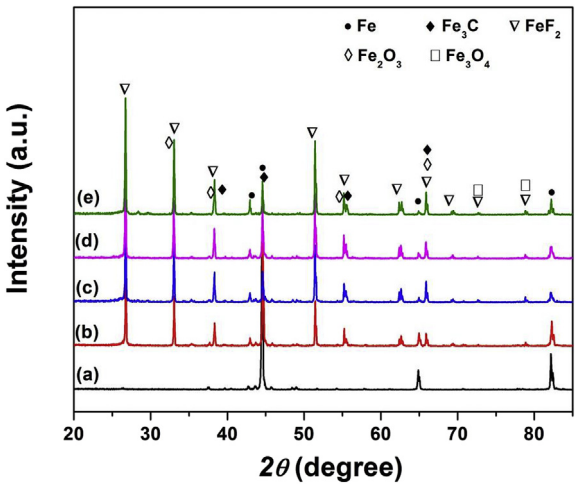

Fig. 2. XRD patterns of F-MCs used in this study. (a) ~ (e) are represented as F-MC-0, F-MC-33, F-MC-50, F-MC-66, F-MC-100, respectively. (A colour version of this figure can be viewed online.)

functionalities were synthesized on the surface of F-MCs. With increase the PVDF loading from 33 wt% to 100 wt% in the precursor, the ionic C-F bonding increased from 37.0 to 43.9%. Semi-ionic C-F and C-F covalent bonding displayed a fluctuation within a narrow range with the increase of PVDF.

Fig. 4 presents the high-resolution XPS C1s spectra with peak deconvolution of F-MCs. Six components were deconvoluted as sp2 carbon (284.4 eV), sp3 carbon (285.2 eV), C–O (286.4 eV), C=O (287.9 eV), O–C=O (e.g. carbonyl and carboxylic: 289.7 eV), and π^* interaction (290.9 eV) [36,39,42]. It was noted that an additional weak intensity peak at 288.9 ± 0.2 eV was obtained in all the F doped samples, which was reported as C-F bond. The quantitative analysis of C 1s spectra was summarized in Table 2. The slight decrease of sp2 carbon content with the increasing of fluorine doping content was observed. The phenomenal might be attributed to the incorporation of fluorine atoms into the carbon skeleton, which causes the structural deformation or lowers the degree of sp2 bonding of the carbon structure, causing more defects (sp3 carbon) [39].

Fig. 5 shows the Raman spectra of F-MCs. The introduction of F heteroatoms into the carbons can significantly vary the adsorbents architecture, causing high disorder degree in the graphene sheets [43]. Therefore, the deconvolution of Raman result was conducted

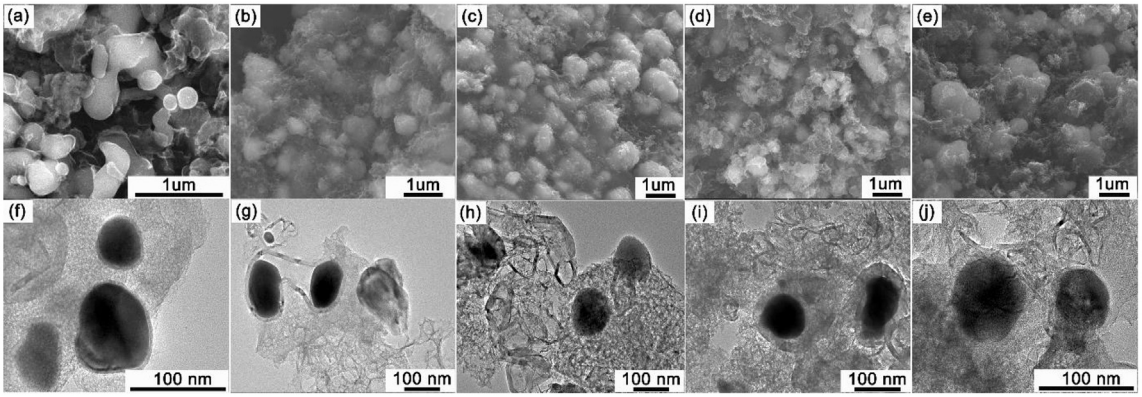

Fig. 1. SEM (a to e) and TEM (f to j) images of magnetic adsorbents: (a and f) for F-MC-0; (b and g) for F-MC-33; (c and h) for F-MC-50; (d and i) for F-MC -66; and (e and j) for F-MC-100.

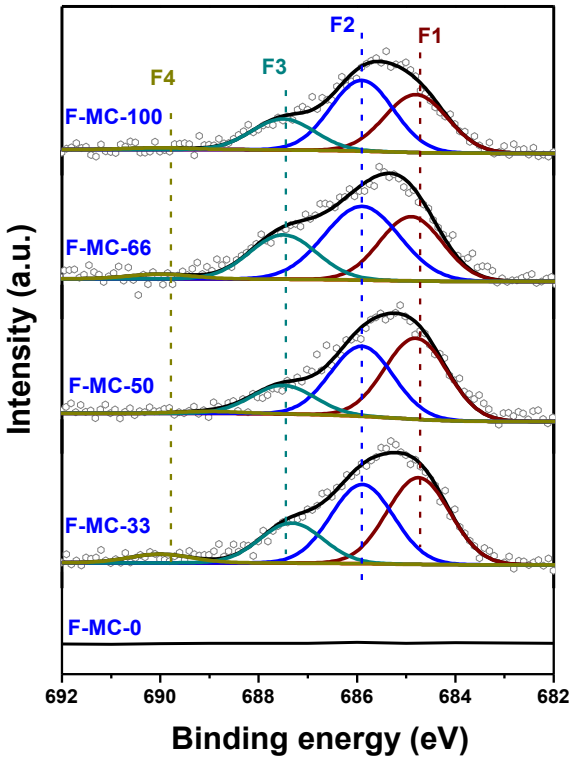

Fig. 3. F_{1s} XPS spectra of the F-MCs. (A colour version of this figure can be viewed online.)

Table 1
Quantitative XPS analysis of the F-MCs and deconvolution of F functionalities: FeF_2 (F1), ionic C-F bond (F2), semi-ionic C-F bond (F3) and covalent C-F bond (F4).

Magnetic Carbons	C [at%]	O [at%]	F [at%]	Fe [at%]	Deconvoluted F_{1s} [%]			
					F1	F2	F3	F4
F-MC-0	87.0	10.8	0	2.2	–	–	–	–
F-MC-33	91.5	6.5	0.9	1.1	40.4	37.0	18.6	4.0
F-MC-50	90.8	6.5	1.7	1.0	44.6	38.6	15.7	1.1
F-MC-66	90.4	6.4	2.1	0.7	31.4	43.2	23.1	2.3
F-MC-100	89.1	6.5	2.5	1.0	35.9	43.9	19.1	1.1

to figure out the variation of the defect degree based on the F doping [43]. Five peaks in Raman results were fitted for each sample, such as I (1166 cm^{-1}), D (1320 cm^{-1}), D" (1490 cm^{-1}), D' (1600 cm^{-1}) and G (1560 cm^{-1}) bands [44]. The intensity ratio of D to G band (I_D/I_G) was used to evaluate the defect degree of F-MCs. The F-MC-0 displayed sharp and narrow peak width with the I_D/I_G value of 0.12, which was also observed in the Fe_3O_4@C nanospheres synthesized by hydrothermal reaction using $Fe(NO_3)_3$ and glucose as precursor [45]. In this work, the I_D/I_G ratio gradually increased from 1.14 to 1.21 with increasing the fluorine content from 0.9% to 2.5% for the fluorine doped samples (Table 1). Since the C-F bonds usually emerged at the vacancies, free edges, or domain boundaries, thus greatly caused higher I_D/I_G value [46,47]. These results demonstrated that the defect degree of the samples could be modulated by the PVDF loading.

The specific surface area (SSA), pore volume and size distribution also play significant roles on the metal ions adsorption, greatly affecting the interaction between the contaminant and active sites [15,16]. The N_2 adsorption-desorption isotherms and pore size distribution of the F-MCs are shown in Fig. 6 and the results are summarized in Table 3. The type-IV adsorption-desorption isotherm curves of all the samples displayed typical property of mesoporous materials. N_2-BET surface area, pore volume and pore size based on the F doped samples were much larger than the un-doped sample (F-MC-0). The highest SSA was 121.6 $m^2\ g^{-1}$ (F-MC-100), 6 times larger than that of the un-doped one (F-MC-0, 21.7 $m^2\ g^{-1}$). Similar result was observed in the pore volume of F-MCs, with 0.28 $cm^3\ g^{-1}$ in F-MC-100, 6 times higher than the F-MC-0. It is worth noting that the SSA of F-MCs gradually increased with increasing the PVDF concentration in precursor, since the incorporation of F dopant into the carbon skeleton can efficiently create more mesoporous carbons, contact surface sites and change the morphologies of carbon adsorbents during the carbonization process [47].

3.2. Cr(VI) removal

The Cr(VI) removal performance and comparison based on various adsorbents are summarized in Table 4. All the samples exhibited good removal capacities for the Cr(VI) removal with an initial Cr(VI) concentration at 40 mg L^{-1} within 10 min. The un-doped sample displayed relatively low efficiency in the Cr(VI) removal, 15.8% removal and 0.44 mg g^{-1} min^{-1}. The doping of F heteroatoms apparently enhanced the Cr(VI) removal performance. With the increase of F content (from 0.9 to 2.5 atom%, see Fig. 3 and Table 1) in the F-MC, the Cr(VI) removal percentage was greatly improved to 100%. The F-MC displayed highest removal efficiency with a mass adsorption ability of 5.9 mg g^{-1} min^{-1}, about 3 times higher than the undoped one (MC). This removal capacity of F-MC was much comparable with state-of-the-art magnetic adsorbent reported before, such as magnetic carbon, N-doped porous carbon and surface modified adsorbents (see Table 4, entries 4–6) [1,22,24], indicating the enhancement of adsorption ability based on F functionalities on the surface of adsorbents.

The magnetic carbons are usually combined with mesoporous carbons and metal particles (Fe, Ni, et al.) [15,16,49]. In this work, F-MC obviously has ZVI nanoparticles on their surface (Fig. 2). Our previous work has revealed that ZVI and produced Fe^{2+} particles played an important role in the Cr(VI) removal, since the redox reaction took place between the Fe^{2+} particles and Cr(VI) ions, which could be presented as Equations (4)–(6) [1,48]:

$$Fe^0 + H^+ \rightarrow Fe^{2+} + R\ (e^-_{aq} \text{ and/or } H^\bullet) \quad (4)$$

$$Cr(VI) + R \rightarrow Cr(III) \quad (5)$$

$$Cr(VI) + Fe^{2+} \rightarrow Cr(III) + Fe^{3+} \quad (6)$$

It may be claimed that the great performance of Cr(VI) removal based on F-MC was simply achieved by the redox between the Fe^{2+} particles and Cr(VI). To exclude this speculation, F-MC was washed by using concentrated HCl for 4 h to eliminate all the metal particles on the surface of adsorbent, noted as F-MC-w (Table 4, entry 3). 87.4% removal percentage was still obtained, demonstrating that the ZVI nanoparticles and Fe^{2+} particles on the surface were not the dominant factor for the Cr(VI) removal in the neutral solution.

From the above discussion, F-MC was the best adsorbent for the Cr(VI) removal, which was chosen as the model adsorbent for further investigations. As shown in Fig. 7a, a rapid Cr(VI) removal performance was observed for the F-MC with Cr(VI) concentration at 70 mg g^{-1}. Almost 53% Cr(VI) removal percentage was obtained within 2.5 min. When the treatment time was prolonged to > 5 min, the removal rate of Cr(VI) ions then became slower, demonstrating that the active sites might be gradually covered by metal ions and thus caused adsorption saturation [1]. The pH value of solution was noticed to great influence the heavy metal removal

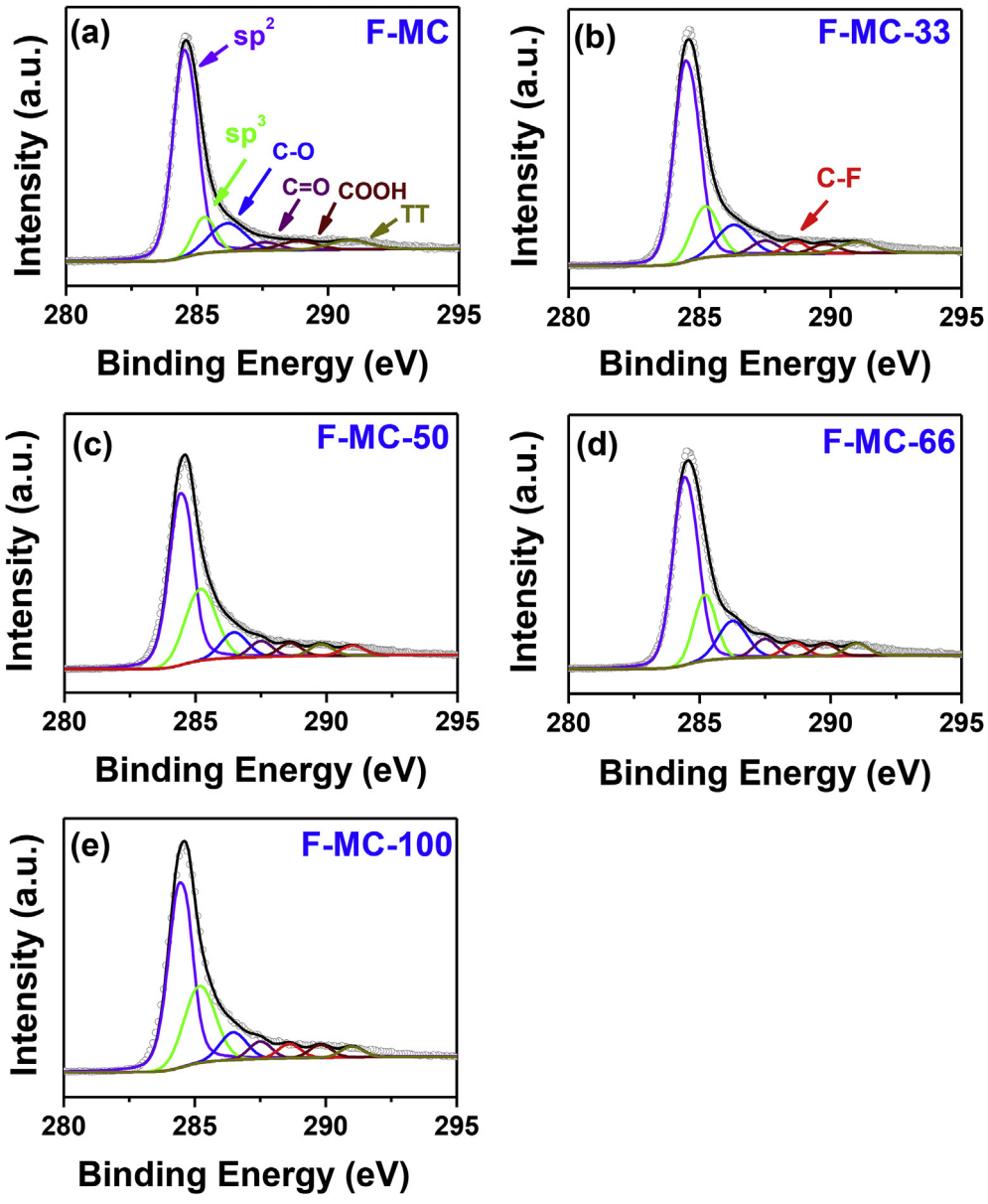

Fig. 4. C_{1s} XPS spectra of the F-MCs. (A colour version of this figure can be viewed online.)

Table 2
Quantitative XPS analysis of the deconvoluted C 1s.

	Deconvoluted C_{1s} [%]						
	sp2 carbon	sp3 carbon	C-O	C=O	C-F	COOH	π*
F-MC-0	68.2	9.3	11.5	2.8	–	3.9	4.3
F-MC-33	61.5	14.4	10.7	3.8	2.9	2.7	3.9
F-MC-50	59.4	16.4	10.2	4.2	2.4	3.7	3.7
F-MC-66	58.8	15.9	11.6	4.3	3.4	3.0	3.0
F-MC-100	54.8	24.9	7.6	4.0	3.3	2.9	2.5

[1,16]. In this work, pH value ranged from 1 to 11 with an initial Cr(VI) concentration of 1000 mg L^{-1} and adsorbent dosage at 2.5 g L^{-1} were studied (Fig. 7b). The 100% Cr(VI) removal percentage was obtained when the pH was lower than 2, indicating that the acid medium had the positive effect on the Cr(VI) removal. Increasing the pH from 3 to 11, the Cr(VI) removal efficiency gradually decreased, from 85.99% to 24.88%, displaying that the Cr(VI) removal efficiency was hindered under the alkaline environment [1]. In fact, several kinds of anionic forms of Cr(VI) ions existed in the aqueous solutions, for instance, chromate (CrO_4^{2-}), dichromate ($Cr_2O_7^{2-}$) and hydrogen chromate ($HCrO_4^-$) [16]. It was well known that in a pH value below 6.8, $HCrO_4^-$ existed as the main ions; and higher pH favored the CrO_4^{2-} oxyanion [24]. The great removal performance of F-MC-100 for the Cr(VI) removal at acidic circumstance can be attributed to two aspects: a) The dissolved ZVIs by acidic solution were much more easily set to produce the intermediates, for example H^+ and Fe^{2+}, which could be used as reactant for the reduction of Cr(VI) ions to Cr(III) [1]; b) The F dopant in the surface might react with Cr(VI) and form the covalent bond [24]. In addition, the electrostatic adsorption between the Cr(VI) ions and the active sites on the surface of F-MC would enhance the adsorption behavior [25].

The Cr(VI) removal performances with different Cr(VI) concentrations by F-MC in the neutral and acidic solution (pH at 1) are shown in Fig. 7c and d, respectively. In the neutral solution, Cr(VI)

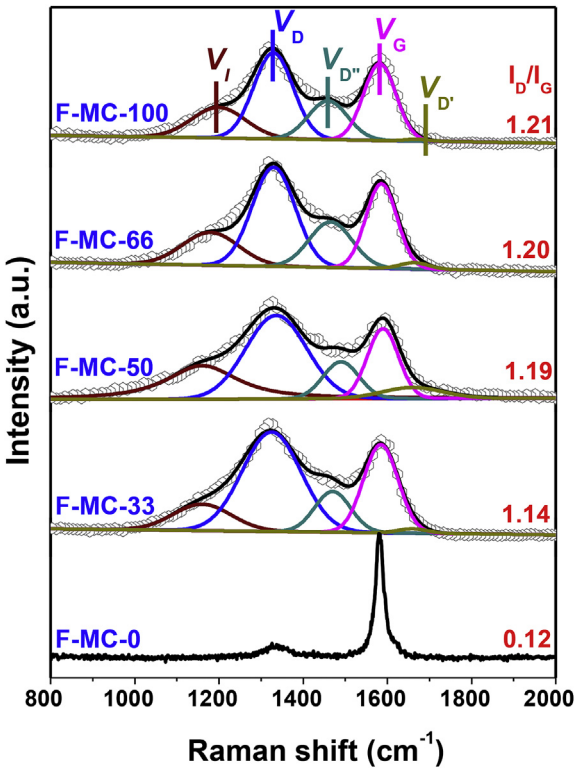

Fig. 5. Raman spectra of F-MCs used in this work. (A colour version of this figure can be viewed online.)

solution with 40 mg L^{-1} could be completely removed by 2.5 g L^{-1} F-MC within 10 min, attributing to the abundant active sites to attract heavy metal ions on the F-MC surfaces. When the Cr(VI) concentration increased to 70 mg L^{-1}, a decline trend was observed, mainly due to the limited active adsorption sites covered by Cr(VI) ions on the surface of the adsorbents [1]. The removal capacity increased alone with increasing the initial Cr(VI) concentration. This can be ascribed to the enhanced driving force by the high initial Cr(VI) concentration, enabling more collisions between the Cr(VI) ions and active sites. Therefore the active sites were gradually saturated with adsorbed Cr(VI) or produced Cr(III) ions [16,25]. When the pH value was adjusted to 1, the activity of F-MC was greatly improved, due to abundance of protons (H^+), which could enhance the redox reaction between the Fe^{2+} particles and Cr(VI) ions [16]. The Cr(VI) ions were totally removed even when the initial Cr(VI) concentration was 2300 mg L^{-1}. And also, similar removal capacity tendency was also observed in the acidic solutions.

3.3. Kinetic study and adsorption isotherms of Cr(VI) over F-MC

Two kinetic models (i.e., pseudo-first-order and pseudo-second-order models) were employed in this work (Fig. S2). The fitting followed a pseudo-second-order model with R^2 more than 0.99, indicating a chemical adsorption for the F-MC adsorbents [50]. The Cr (VI) ions adsorption isotherms fitted by Langmuir and Freundlich models were conducted for the F-MC in the neutral and acidic solutions (Fig. S3 and Table S1). Two models were used for the fittings. Based on the correlation coefficient values and the R^2 value, it can be seen that the adsorption linear isotherm by Langmuir model fits superior to the Freundlich model. The calculated maximum adsorption capacities of adsorbents by the Langmuir model were 48.78 and 1423.4 mg g^{-1} in neutral and acidic solution, respectively, much higher than the reported adsorbent so far and displaying a competitive activity with the state-of-the-art surface modified and magnetic adsorbents, such as surface functionalized PAN fibers, CNT core-in-hematite shell capsules and activated carbon [51–53], even though these adsorbents have higher SSA (see Table 5). To verify the reasonableness of the obtained q_{max}, the adsorption isotherms in a non-linear plot of C_e vs. q_e were carried out in neutral and acid solutions. As shown in Fig. S4 and Table S2, the calculated q_{max} were 35.3 and 970.8 mg g^{-1} in neutral and acidic solution, respectively, a little lower than the obtained results from linear-isotherm. Meanwhile, for the Langmuir adsorption isotherm, the value of R^2 (0.81 and 0.92, non-linear fitting in neutral and acid solution) is lower than that of R^2 (0.95 and 0.94, linear fitting in neutral and acid solution). These results demonstrated that the linear method is a better way to obtain the adsorption parameters for our experiment, which is the reverse of the literature conclusion [54–56]. The reason for this result is that the process of Cr(VI) removal over F-MC is more complicated, involving of redox reaction and adsorption. And the redox reaction plays significant role in this process [1,15,30]. The driving force from the electrostatic attraction for the Cr(VI) ions on the surface of adsorbent was also enhanced by the fluorine doping. Therefore, such excellent activities on the Cr(VI) removal can be attributed to the much more active sites over F-MC, resulting in the enhancement for the Cr(VI) ions adsorption.

3.4. Stability

The F-MC also shows desired stability in the Cr(VI) removal. After each run, the recycled adsorbent was washed by deionized water and 0.01 mol L^{-1} NaOH solution repeatedly several times for the adsorbent regeneration [61,62]. The collected solid was then dried at 80 °C overnight. Fig. 8 shows the stability of the F-MC in the Cr(VI) removal during five recycling tests. A very small decline in the Cr(VI) removal was observed after each test. Nevertheless, about 93.6% removal percentage of Cr(VI) and 15 mg g^{-1} removal capacity after the 5th cycle were still obtained. Moreover, as shown in Fig. S6, compared with the fresh F-MC, the morphology and surface defects were unchanged apparently after 5 recycles, indicating that the F-MC have an high stability for the Cr(VI) removal under the mild conditions. Nevertheless, the magnetism of the treated sample decreased, ascribed to the consumption of ZVI particles on the surface of adsorbent. In addition, compared with the fresh sample, the F_{1s} XPS spectra of the recycled F-MC showed that the F functionalities were covered by the Cr(VI) or produced Cr(III) ions after treatment (Fig. S7).

3.5. Cr(VI) removal mechanism

To investigate the mechanism of Cr(VI) removal over F-MCs, the relationships between the Cr(VI) removal efficiency with the physical- and chemical-property as well as the structure were discussed in detail. According to the previous work, there was a chemical redox reaction for the Cr(VI) ions to produce Cr(III) ions in this system, which was very important for the Cr(VI) removal [1,16,22]. ZVI was reported to play a significant role in the magnetic carbon-Cr(VI) removal system. The low pH value can effectively improve the Cr(VI) removal, because of the participation of more H^+ ions in the system [64]. Nevertheless, very low removal performances were obtained in the neutral solution or low pH solution (pH value at 2–3) with undoped magnetic carbons or sole nitrogen doped magnetic carbons as adsorbent (see Table 4). Therefore, there was a certain significant factor such as F dopant, which can dramatically increase the Cr(VI) ions removal performance. From the Table 1 and Fig. 1, the results evidenced that the activities of F-

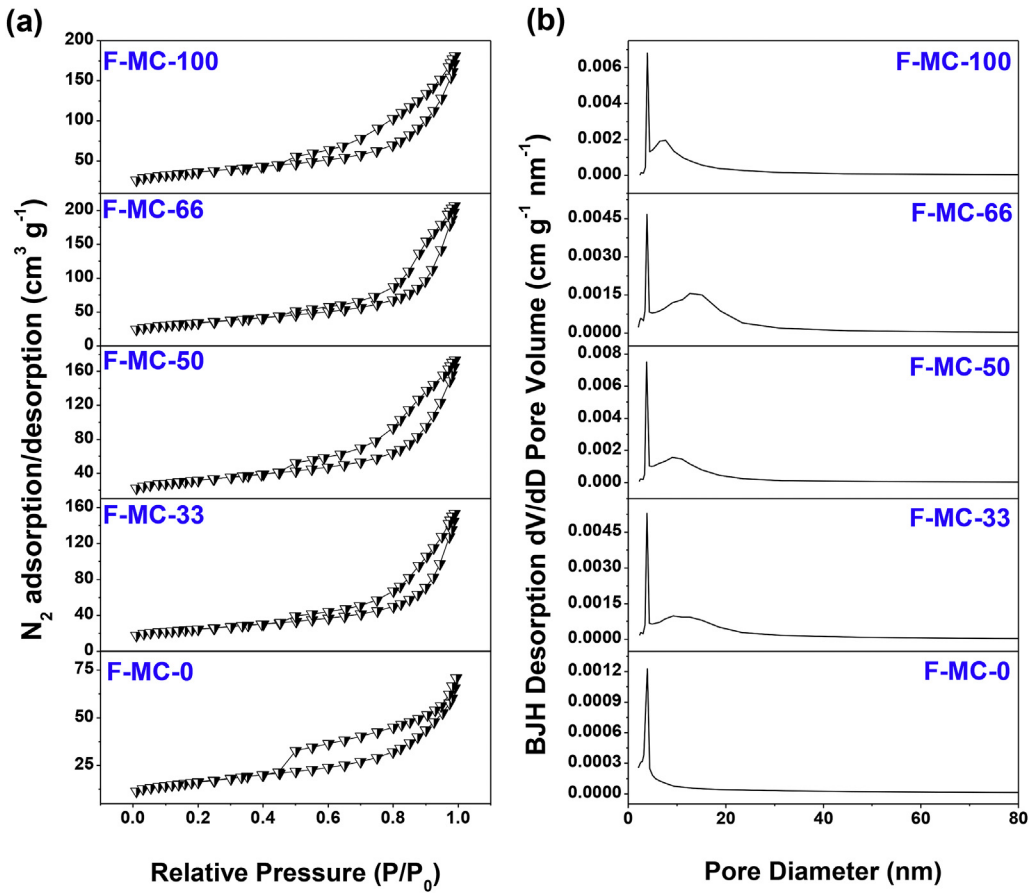

Fig. 6. N_2 adsorption–desorption isotherms and pore size distribution of F-MCs used in this work. (A colour version of this figure can be viewed online.)

Table 3
BET SSAs, pore volume (PV) and average pore size (APZ) of the fluorine doped magnetic carbons.

	F-MC-0	F-MC-33	FMC-50	FMC-66	F-MC-100
SSA ($m^2\ g^{-1}$)	21.7	84.4	108.0	116.5	121.6
PV(10^{-2}) ($cm^3\ g^{-1}$)	4.6	23.7	26.8	31.9	28.0
APZ (nm)	9.6	13.5	11.7	13.2	11.8

MC could be enhanced by the introduction of F dopant, indicating that the physical- and chemical- property can be changed by the F dopant. The distinct activity of F-MC for the Cr(VI) removal propelled us to find the essential factors on the structure-performance relationship of the F-MCs with different F doping levels and architecture in the Cr(VI) removal in the neutral solution. As the adsorption and redox occurred on the surface of magnetic carbons, the surface-area-normalized removal rates were utilized to evaluate the removal performance in this study.

The Cr(VI) removal performances of F-MCs are summarized in

Table 4
The performance comparison of different adsorbents in the Cr(VI) removal.[a]

Entry	Adsorbent	S_{BET}[b] ($m^2\ g^{-1}$)	X[c] (%)	r_g[d] (mg g^{-1} min^{-1})	r_s[e] (mg m^{-2} min^{-1})
1	MC[f]	21.7	15.8	0.44	0.020
2	F-MC[g]	56.2	100	5.9	0.049
3	F-MC-w[h]	–	87.4	–	–
4	Iron nanoparticles[i]	35.0	100	0.008	7.0×10^{-4}
5	N-doped porous carbon[j]	1136.0	92	0.063	5.6×10^{-5}
6	PEI/CF[k]	1622.4	100	0.018	1.1×10^{-5}

[a] Condition: [Cr (VI)] = 40 mg L^{-1}, pH = 7.0, adsorbent dosage: 50.0 mg, volume: 20 mL, treatment time: 10 min.
[b] BET surface area.
[c] X: removal percentages.
[d] Removal rate of Cr(VI) per gram of adsorbent within 2.5 min.
[e] Removal rate of Cr(VI) per m^2 of adsorbent surface based on the ultrasonic treatment with 2.5 min.
[f] MC is represented as F-MC-0.
[g] F-MC is represented as F-MC-100.
[h] Washed by concentrated HCl for 4 h.
[i] Condition: [Cr (VI)] = 42.83 ± 0.52 mg L^{-1}, pH = 11.0 ± 0.5, adsorbent dosage: 60.0 mg, volume: 40 mL, treatment time: 10 min (ref. [48]).
[j] Condition: [Cr (VI)] = 31.73 mg L^{-1}, pH = 3, adsorbent dosage: 2 g L^{-1}, treatment time: 10 min (ref. [24]).
[k] PEI/CF is carbon fiber coated with polyethylenimine. Condition: [Cr (VI)] = 2 mg L^{-1}, pH = 1.0, adsorbent dosage: 2.25 g L^{-1}, treatment time: 45 min (ref. [21]).

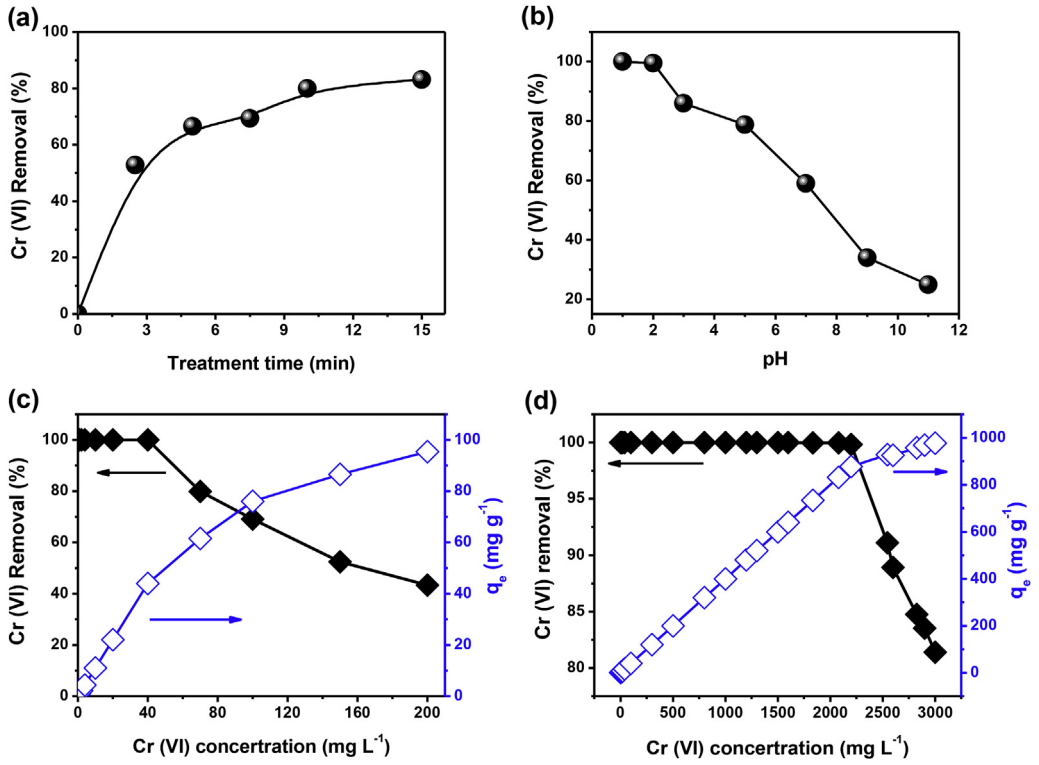

Fig. 7. (a) Cr(VI) removal performance with different treatment time ([Cr (VI)] = 70 mg L^{-1}, pH = 7, adsorbent dosage: 50.0 mg, volume: 20 mL); (b) Effect of solution pH on the Cr(VI) removal efficiency. ([Cr(VI)] = 1000 mg/L, adsorbent dosage: 50.0 mg, volume: 20 mL, treating time: 10 min); the effect of initial Cr(VI) concentration with pH at 7 (c) and 1 (d) (adsorbent dosage: 50.0 mg, volume: 20 mL, treating time: 10 min). (A colour version of this figure can be viewed online.)

Table 5
Comparison of Cr(VI) adsorption capacities with other adsorbents.

	Adsorbent	S_{BET} (m^2 g^{-1})	q_{max}[a] (mg g^{-1})	q_s[b] × 10^2 (mg m^{-2})	pH	Refs.
Neutral solution	F-MC	121.6	48.78	40.1	7	This work (linear)
		121.6	35.3	40.1	7	This work (non-linear)
	Magnetic Carbon (Cellulose)	111.4	15.3	13.7	7	[1]
	MN (Cotton fabric)	91.1	3.74	4.1	7	[16]
	Graphene nanocomposites	42.1	1.03	2.4	7	[57]
Acidic solution	F-MC	273.4[c]	1423.4	520.6	1	This work (linear)
		273.4[c]	970.8	355.1	1	This work (non-linear)
	PEI/ECs	–	36.8	–	3	[21]
	PANI/CFs	1017.3	18.1	1.8	1	[22]
	CNT core-in-hematite shell capsules	270	29.16	0.1	5	[51]
	PAN-NH2 nanofibers	–	137.6	–	2	[58]
	PEI-modified aerobic granular sludge	–	348.1	–	5.2	[59]
	MRT	628.0	102.88	16.4	3	[28]
	Surface functionalized PAN fiber	–	20.7	–	2.5	[52]
	Surface modified tannery residual biomass	–	177–217	–	2	[60]
	Activated carbon	–	112.36	–	1	[53]
	PAN/Ppy core shell nanofibers	–	74.9	–	2.0	[61]
	MnO_2/Fe_3O_4/o-WCNTs	92.0	186.9	203.2	2	[62]
	α-Fe_2O_3	40.0	4.47	11.2	3	[63]
	N doped porous carbon (Fe)	1136.0	16	2.6	3	[24]
	N-doped porous carbon (Ni)	2148.4	96.27	4.5	2.5	[25]

[a] q_{max} is obtained through the Langmuir isotherm.
[b] q_s is represented as the adsorption capacity per m^2 of catalyst surface.
[c] The SSA of treated F-MC in acid solution. The result was obtained from Fig. S5.

Table 6. The Cr(VI) removal efficiency with an initial Cr(VI) concentration at 70 mg g^{-1} increased with increasing the F content (Fig. 3 and Table 1), from 5.84% to 79.92% removal within 10 min. The highest efficiency for the Cr(VI) removal was obtained on the F-MC-100. Generally speaking, larger BET surface area and bigger pore size can improve the Cr(VI) diffusion into the internal pores and facilitate the redox reaction between the electron donors (ZVI or Fe^{2+} particles) and Cr(VI) ions, thus enhancing the removal efficiency (Table 3, Fig. 9a) [1]. To exclude the structure dependence of adsorbents, the removal rate normalized by mass weight and surface area were applied to represent the Cr(VI) removal efficiency of F-MC. As revealed in Table 6, the removal rates based on the dose and specific surface areas of adsorbents also increased with the increase of the F doping level. The highest removal activities,

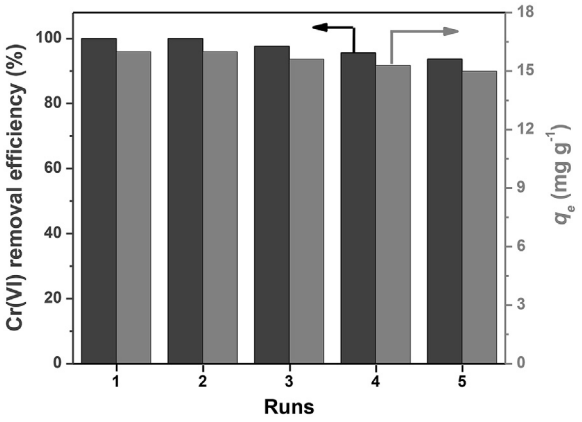

Fig. 8. The reusability of the F-MC for the Cr(VI) removal in this work. Condition: [Cr (VI)] = 40 mg L^{-1}, pH = 7.0, adsorbent dosage: 50.0 mg, volume: 20 mL, treatment time: 10 min.

Table 6
The performance of F-MCs in the Cr(VI) removal.[a]

Entry	Adsorbent	X[b] (%)	r_g[c] (mg g^{-1} min^{-1})	r_s[d] (mg m^{-2} min^{-1})
1	F-MC-0	5.84	0.48	0.022
2	F-MC-33	25.11	2.36	0.028
3	F-MC-50	58.20	4.31	0.040
4	F-MC-66	74.17	5.49	0.047
5	F-MC-100	79.92	5.92	0.049

[a] Condition: [Cr (VI)] = 70 mg L^{-1}, pH = 7.0, adsorbent dosage: 50.0 mg, volume: 20 mL, treatment time: 10 min.
[b] X: removal percentages.
[c] Removal rate of Cr(VI) per gram of adsorbent within 2.5 min.
[d] Removal rate of Cr(VI) per m^2 of adsorbent surface within 2.5 min.

5.92 mg g^{-1} min^{-1} and 0.049 mg m^{-2} min^{-1}, were obtained over the adsorbent synthesized from PVDF. These results evidenced that the removal performance of F-MCs can be modulated by the fluorine doping levels.

Heterogeneous atoms were usually considered as the active sites in many fields, such as hydrocarbon oxidation, electrochemistry and photocatalysis [42,47,65–70]. In the case of Cr(VI) removal, the nitrogen heterogeneous dopant has been reported to play a significant role in the enhancement of Cr(VI) removal [23–25,29,49]. In this work, we speculated that the F dopants also can adjust electron density in the surface of F-MC. Meanwhile, F atom has a higher electronegativity than N atom [71], indicating that the F dopant also can be used as the active sites in the heavy metal removal. From the dependence of the defects (I_D/I_G) and removal rate, as shown in Fig. 9b, it can be clearly observed that the defects can improve the Cr(VI) removal efficiency, indicating that the F dopants at edges may be used as active sites in the heavy metal removal, since the F dopant emerged at edges [36]. In order to uncover the influence of F dopant, the dependences of surface-area-normalized removal efficiency on the fluorine gross content and functionalities content in F-MCs were investigated in detail. The fluorine contents of each adsorbent were measured by XPS (see Fig. 3 and Table 1). From Fig. 10, the gross F doping and two specific types of the F functionalities on the surface of magnetic carbons were correlated with the removal rate and a positive effect of fluorine functionalities in the Cr(VI) removal was observed. The content of covalent C-F bond was negligible to fitted the relationship with Cr(VI) removal efficiency (Table 1). Nevertheless, based on our current work, to distinguish the separate role of the specific functionality on the Cr(VI) removal rate is still a challenge, since these four kinds of fluorine functionalities increased alone with increasing the gross fluorine content simultaneously during the carbonization of PVDF in this work.

According to the previous work, the redox reaction between the Cr(VI) ions and Fe^{2+} particles occurred in the Cr(VI) removal, indicating that the consumption of iron from F-MCs is inevitable. In fact, the enhancement of Cr(VI) removal performance in the acidic circumstance can be attributed to the boosting of redox reaction between Cr(VI) ions and the Fe^{2+} particles on the adsorbents surface. To investigate the effect of redox reaction on the surface of adsorbent, the F doped adsorbents before and after treated in the neutral solution were characterized. The element of Cr and Fe were detected on the F-MC surface by XPS (Fig. S8). Fig. 11a shows the Cr_{2p} XPS spectra of F-MC after treated in the neutral solution. The Cr_{2p} curve was deconvoluted into four components, peaks at 577.5, 587.2, 579.0 and 589.2 eV attributing to Cr(VI) and Cr(III), respectively, indicating that the Cr(VI) ions were partly reduced to Cr(III) ions based on the redox reaction [24]. The oxygen-containing functionalities on the surface were also investigated, since the functional group on the adsorbents surface could also react with

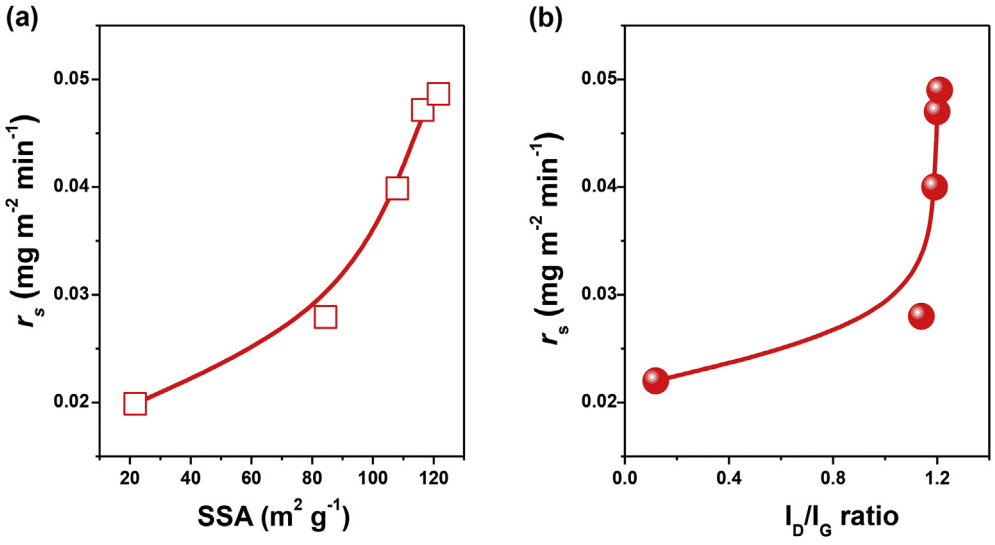

Fig. 9. Dependence of Cr(VI) removal rate on the SSA surface area (a) and defect degree (b) of F-MCs. (A colour version of this figure can be viewed online.)

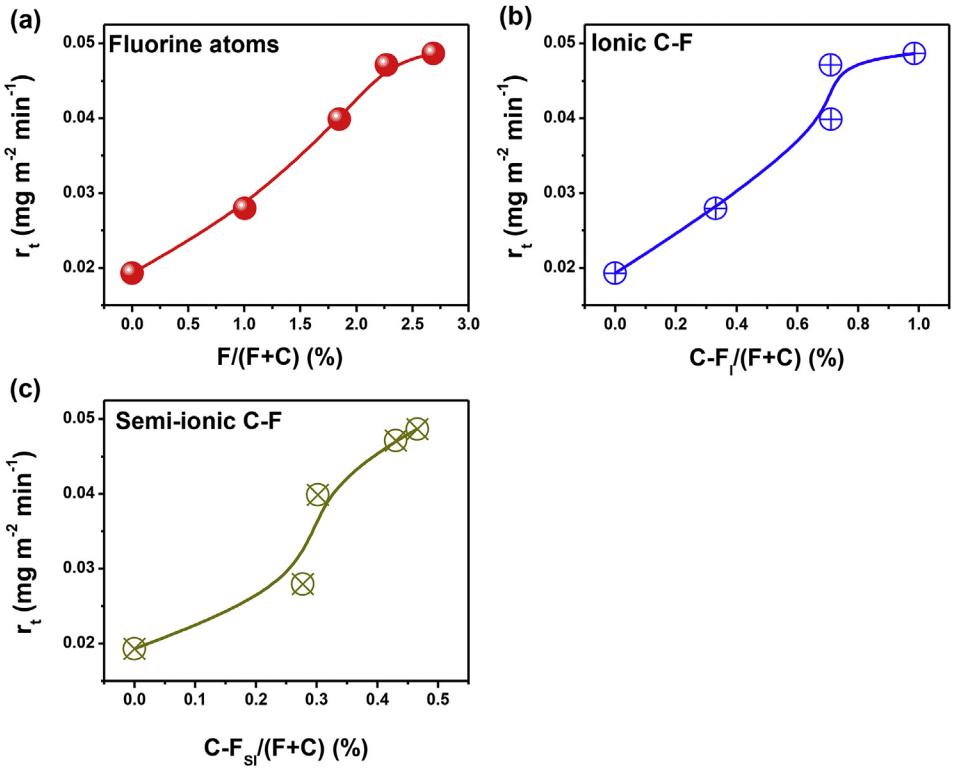

Fig. 10. Relationship between Cr(VI) removal rate and the amounts of fluorine functionalities on F-MCs: (a) gross F and the deconvoluted F (ionic C-F bonding (b) and semi-ionic C-F bonding (c). (A colour version of this figure can be viewed online.)

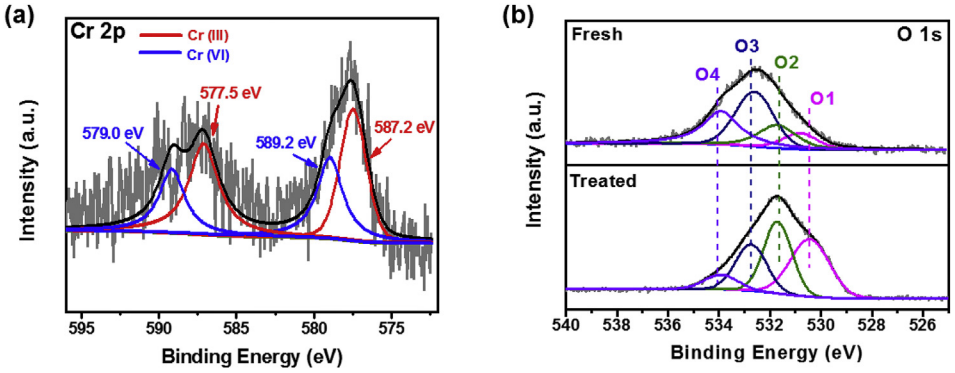

Fig. 11. (a) Cr_{2p} XPS spectral of treated F-MC, (b) O 1s XPS spectral of the fresh and after treated F-MC. (A colour version of this figure can be viewed online.)

Cr(VI) ions in the solution [64]. Fig. 11b shows the O_{1s} XPS spectra of the fresh and the 5th recycled F-MC. Four peaks at 530.7, 531.7, 532.8 and 533.6 eV were attributed to quinonic C=O (O1), ketonic C=O (O2), etherlike C–O–C (O3) and hydroxyl C–OH (O4) groups, respectively [72]. It can be seen that after treatment, the content of oxygen containing groups, such as quinonic C=O and ketonic C=O, were greatly increased, indicating that the carbons surface was oxidized by the Cr(VI) ions with more oxygen species and Cr(III) ions produced [64]. The oxidation reaction could be abbreviated by Equation (7):

$$HCrO_4^-(aq.) + \text{Carbons (s)} \rightarrow Cr^{3+}(aq.) + \text{Carbons-O (s)} \quad (7)$$

Hence, Cr(VI) ions reacted with the carbon species and were reduced to Cr(III) ions eventually, which were attached on the surface of F-MC in this process, subsequently (Fig. 11a). Furthermore, researchers such as Gu and Hu have reported that the oxygen containing groups (e.g. carboxyl group) were proved to enhance the removal capacity in the Cr(VI) removal [64,73]. The interaction between the Cr(VI) ions and oxygen containing groups can be attributed to surface complexation. However, in current work, it is hard to exclude the effect of oxygen containing groups, since it combines the adsorption and redox reaction in the Cr(VI) removal [1,30]. To this end, the controllable synthesis of F doped carbons with a known content of oxygen containing group is desirable in the future.

4. Conclusion

In summary, F-MC was synthesized through a one-step pyrolysis method and used as adsorbent in the Cr(VI) removal for the first time. As high as 48.78 and 1423.4 mg g^{-1} removal capacities for the

Cr(VI) removal in the neutral and acidic solution were achieved, higher than the state-of-the-art adsorbents such as magnetic carbons, active carbon and surface modified adsorbents in the environment remediation. The higher Cr(VI) removal capacitance was obtained at low pH solution, ascribed to the more involved H^+ ions for the redox reaction. F functionalities such as ionic and semi-ionic bonds displayed positive influences on the removal efficiency. Also, the carbon atoms on the adsorbent surface reacted with Cr(VI) to produce Cr(III) ions while more oxygen functionalities increased. These results showed that great Cr(VI) removal performance of F-MC could be attributed to the adsorption and redox reaction, which were greatly enhanced by the F dopant. In addition, the F-MC with demonstrated outstanding recyclability can be applied as the potential adsorbents in the Cr(VI) removal for industrial application.

Acknowledgement

This project was financially supported from the start-up fund of University of Tennessee, National Natural Science Foundation of China (Nos. 21503082, 51573063 and 21174044), Open project of state key lab of organic inorganic composites, Guangdong Provincial National Science Foundation (Nos. 2014A030310447 and S2013020013855) and the China Scholarship Council. Part of the characterizations including the TGA, TEM and XRD were carried out at the Center for Nanophase Materials Sciences in Oak Ridge National Laboratory, which is a DOE Office of Science User Facility.

Appendix A. Supplementary data

Supplementary data related to this article can be found at http://dx.doi.org/10.1016/j.carbon.2017.01.033.

References

[1] B. Qiu, H. Gu, X. Yan, J. Guo, Y. Wang, D. Sun, et al., Cellulose derived magnetic mesoporous carbon nanocomposites with enhanced hexavalent chromium removal, J. Mater. Chem. A 2 (41) (2014) 17454–17462.
[2] Z.-R. Guo, G. Zhang, J. Fang, X. Dou, Enhanced chromium recovery from tanning wastewater, J. Clean. Prod. 14 (1) (2006) 75–79.
[3] C. Wang, X. Hu, M.-L. Chen, Y.-H. Wu, Total concentrations and fractions of Cd, Cr, Pb, Cu, Ni and Zn in sewage sludge from municipal and industrial wastewater treatment plants, J. Hazard. Mater. 119 (1–3) (2005) 245–249.
[4] Y. Xu, D. Zhao, Reductive immobilization of chromate in water and soil using stabilized iron nanoparticles, Water Res. 41 (10) (2007) 2101–2108.
[5] L. Monser, N. Adhoum, Modified activated carbon for the removal of copper, zinc, chromium and cyanide from wastewater, Sep. Purif. Technol. 26 (2) (2002) 137–146.
[6] A.-N.A. El-Hendawy, The role of surface chemistry and solution pH on the removal of Pb^{2+} and Cd^{2+} ions via effective adsorbents from low-cost biomass, J. Hazard. Mater. 167 (1) (2009) 260–267.
[7] K. Kadirvelu, C. Namasivayam, Activated carbon from coconut coirpith as metal adsorbent: adsorption of Cd(II) from aqueous solution, Adv. Environ. Res. 7 (2) (2003) 471–478.
[8] H. Hasar, Adsorption of nickel (II) from aqueous solution onto activated carbon prepared from almond husk, J. Hazard. Mater. 97 (1) (2003) 49–57.
[9] M.A.A. Zaini, R. Okayama, M. Machida, Adsorption of aqueous metal ions on cattle-manure-compost based activated carbons, J. Hazard. Mater. 170 (2) (2009) 1119–1124.
[10] B. Krishna, D. Murty, B.J. Prakash, Surfactant-modified clay as adsorbent for chromate, Appl. Clay Sci. 20 (1) (2001) 65–71.
[11] A.M. Yusof, N.A.N.N. Malek, Removal of Cr(VI) and As(V) from aqueous solutions by HDTMA-modified zeolite Y, J. Hazard. Mater. 162 (2) (2009) 1019–1024.
[12] D. Kratochvil, P. Pimentel, B. Volesky, Removal of trivalent and hexavalent chromium by seaweed biosorbent, Environ. Sci. Tech. 32 (18) (1998) 2693–2698.
[13] A. Szabó, D. Gournis, M.A. Karakassides, D. Petridis, Clay–Aminopropylsiloxane compositions, Chem. Mater. 10 (2) (1998) 639–645.
[14] H. Tamai, T. Kakii, Y. Hirota, T. Kumamoto, H. Yasuda, Synthesis of extremely large mesoporous activated carbon and its unique adsorption for giant molecules, Chem. Mater. 8 (2) (1996) 454–462.
[15] B. Qiu, Y. Wang, D. Sun, Q. Wang, X. Zhang, B.L. Weeks, et al., Cr(vi) removal by magnetic carbon nanocomposites derived from cellulose at different carbonization temperatures, J. Mater. Chem. A 3 (18) (2015) 9817–9825.
[16] J.H. Zhu, H.B. Gu, J. Guo, M.J. Chen, H.G. Wei, Z.P. Luo, et al., Mesoporous magnetic carbon nanocomposite fabrics for highly efficient Cr(VI) removal, J. Mater. Chem. A 2 (7) (2014) 2256–2265.
[17] I.L. Shashkova, A.I. Rat'ko, N.V. Kitikova, Removal of heavy metal ions from aqueous solutions by alkaline-earth metal phosphates, Colloids Surf. A 160 (3) (1999) 207–215.
[18] C.X. Xu, B. Qiu, H.B. Gu, X.R. Yang, H.G. Wei, X.H. Huang, et al., Synergistic interactions between activated carbon fabrics and toxic hexavalent chromium, ECS J. Solid State Sci. Technol. 3 (3) (2014) M1–M9.
[19] J.H. Zhu, S.Y. Wei, M.J. Chen, H.B. Gu, S.B. Rapole, S. Pallavkar, et al., Magnetic nanocomposites for environmental remediation, Adv. Powder Technol. 24 (2) (2013) 459–467.
[20] J.H. Zhu, R. Sadu, S.Y. Wei, D.H. Chen, N. Haldolaarachchige, Z.P. Luo, et al., Magnetic graphene nanoplatelet composites toward arsenic removal, ECS J. Solid State Sci. Technol. 1 (1) (2012) M1–M5.
[21] B. Qiu, J. Guo, X. Zhang, D. Sun, H. Gu, Q. Wang, et al., Polyethylenimine facilitated ethyl cellulose for hexavalent chromium removal with a wide pH range, ACS Appl. Mater. Interfaces 6 (22) (2014) 19816–19824.
[22] B. Qiu, C. Xu, D. Sun, H. Wei, X. Zhang, J. Guo, et al., Polyaniline coating on carbon fiber fabrics for improved hexavalent chromium removal, RSC Adv. 4 (56) (2014) 29855.
[23] F. Cai, X. Liu, S. Liu, H. Liu, Y. Huang, A simple one-pot synthesis of highly fluorescent nitrogen-doped graphene quantum dots for the detection of Cr(vi) in aqueous media, RSC Adv. 4 (94) (2014) 52016–52022.
[24] Y. Li, S. Zhu, Q. Liu, Z. Chen, J. Gu, C. Zhu, et al., N-doped porous carbon with magnetic particles formed in situ for enhanced Cr(VI) removal, Water Res. 47 (12) (2013) 4188–4197.
[25] S. Zhang, X. Wang, J. Li, T. Wen, J. Xu, X. Wang, Efficient removal of a typical dye and Cr(vi) reduction using N-doped magnetic porous carbon, RSC Adv. 4 (108) (2014) 63110–63117.
[26] G. Zhao, L. Jiang, Y. He, J. Li, H. Dong, X. Wang, et al., Sulfonated graphene for persistent aromatic pollutant management, Adv. Mater. 23 (34) (2011) 3959–3963.
[27] A.L. Allred, E.G. Rochow, A scale of electronegativity based on electrostatic force, J. Inorg. Nucl. Chem. 5 (4) (1958) 264–268.
[28] J. Wang, S. Xu, Y. Wang, R. Cai, C. Lv, W. Qiao, et al., Controllable synthesis of hierarchical mesoporous/microporous nitrogen-rich polymer networks for CO_2 and Cr(vi) ion adsorption, RSC Adv. 4 (31) (2014) 16224–16232.
[29] K.-Y. Shin, J.-Y. Hong, J. Jang, Heavy metal ion adsorption behavior in nitrogen-doped magnetic carbon nanoparticles: isotherms and kinetic study, J. Hazard. Mater. 190 (1–3) (2011) 36–44.
[30] Y. Cao, J. Huang, Y. Li, S. Qiu, J. Liu, A. Khasanov, et al., One-pot melamine derived nitrogen doped magnetic carbon nanoadsorbents with enhanced chromium removal, Carbon 109 (2016) 640–649.
[31] X. Sun, P. Song, Y. Zhang, C. Liu, W. Xu, W. Xing, A class of high performance metal-free oxygen reduction electrocatalysts based on cheap carbon blacks, Sci. Rep. 3 (2013) 2505.
[32] J. Zhou, J. Lian, L. Hou, J. Zhang, H. Gou, M. Xia, et al., Ultrahigh volumetric capacitance and cyclic stability of fluorine and nitrogen co-doped carbon microspheres, Nat. Commun. 6 (2015) 8503.
[33] Z. He, Q. Cai, M. Wu, Y. Shi, H. Fang, L. Li, et al., Photocatalytic reduction of Cr(VI) in an aqueous suspension of surface-fluorinated anatase TiO2 nanosheets with exposed {001} facets, Ind. Eng. Chem. Res. 52 (28) (2013) 9556–9565.
[34] Z. He, L. Jiang, D. Wang, J. Qiu, J. Chen, S. Song, Simultaneous oxidation of p-chlorophenol and reduction of Cr(VI) on fluorinated anatase TiO2 nanosheets with dominant {001} facets under visible irradiation, Ind. Eng. Chem. Res. 54 (3) (2015) 808–818.
[35] S. Liu, X. Sun, J.-G. Li, X. Li, Z. Xiu, H. Yang, et al., Fluorine-and iron-modified hierarchical anatase microsphere photocatalyst for water cleaning: facile wet chemical synthesis and wavelength-sensitive photocatalytic reactivity, Langmuir 26 (6) (2009) 4546–4553.
[36] H. Ming, J. Ming, W.-J. Kwak, W. Yang, Q. Zhou, J. Zheng, et al., Fluorine-doped porous carbon-decorated Fe_3O_4-FeF_2 composite versus $LiNi_{0.5}Mn_{1.5}O_4$ towards a full battery with robust capability, Electrochim. Acta 169 (2015) 291–299.
[37] B. Breitung, M.A. Reddy, V.S.K. Chakravadhanula, M. Engel, C. Kübel, A.K. Powell, et al., Influence of particle size and fluorination ratio of CFx precursor compounds on the electrochemical performance of C–FeF2 nanocomposites for reversible lithium storage, Beilstein J. Nanotech. 4 (2013) 705–713.
[38] M.J. Armstrong, A. Panneerselvam, C. O'Regan, M.A. Morris, J.D. Holmes, Supercritical-fluid synthesis of FeF_2 and CoF_2 Li-ion conversion materials, J. Mater. Chem. A 1 (36) (2013) 10667–10676.
[39] G. Panomsuwan, N. Saito, T. Ishizaki, Simple one-step synthesis of fluorine-doped carbon nanoparticles as potential alternative metal-free electrocatalysts for oxygen reduction reaction, J. Mater. Chem. A 3 (18) (2015) 9972–9981.
[40] H. Geng, Q. Zhou, Y. Pan, H. Gu, J. Zheng, Preparation of fluorine-doped, carbon-encapsulated hollow Fe_3O_4 spheres as an efficient anode material for Li-ion batteries, Nanoscale 6 (7) (2014) 3889–3894.
[41] J. Giraudet, C. Delabarre, K. Guérin, M. Dubois, F. Masin, A. Hamwi, Comparative performances for primary lithium batteries of some covalent and semi-covalent graphite fluorides, J. Power Sources 158 (2) (2006) 1365–1372.
[42] Y.H. Cao, X.Y. Luo, H. Yu, F. Peng, H.J. Wang, G.Q. Ning, sp^2- and sp^3-hybridized

carbon materials as catalysts for aerobic oxidation of cyclohexane, Catal. Sci. Tech. 3 (2013) 2654–2660.
[43] Y. Cao, H. Yu, J. Tan, F. Peng, H. Wang, J. Li, et al., Nitrogen-, phosphorous-and boron-doped carbon nanotubes as catalysts for the aerobic oxidation of cyclohexane, Carbon 57 (2013) 433–442.
[44] S. Maldonado, S. Morin, K.J. Stevenson, Structure, composition, and chemical reactivity of carbon nanotubes by selective nitrogen doping, Carbon 44 (8) (2006) 1429–1437.
[45] N. Zhao, S. Wu, C. He, Z. Wang, C. Shi, E. Liu, et al., One-pot synthesis of uniform Fe3O4 nanocrystals encapsulated in interconnected carbon nanospheres for superior lithium storage capability, Carbon 57 (2013) 130–138.
[46] J.T. Robinson, J.S. Burgess, C.E. Junkermeier, S.C. Badescu, T.L. Reinecke, F.K. Perkins, et al., Properties of fluorinated graphene films, Nano Lett. 10 (8) (2010) 3001–3005.
[47] Y.H. Cao, H. Yu, J. Tan, F. Peng, H.J. Wang, J. Li, et al., Nitrogen-, phosphorous-and boron-doped carbon nanotubes as catalysts for the aerobic oxidation of cyclohexane, Carbon 57 (2013) 433–442.
[48] J. Cao, W.-X. Zhang, Stabilization of chromium ore processing residue (COPR) with nanoscale iron particles, J. Hazard. Mater. 132 (2–3) (2006) 213–219.
[49] A. Modi, B. Bhaduri, N. Verma, Facile one-step synthesis of nitrogen-doped carbon nanofibers for the removal of potentially toxic metals from water, Ind. Eng. Chem. Res. 54 (18) (2015) 5172–5178.
[50] J.H. Zhu, H.B. Gu, S.B. Rapole, Z.P. Luo, S. Pallavkar, N. Haldolaarachchige, et al., Looped carbon capturing and environmental remediation: case study of magnetic polypropylene nanocomposites, RSC Adv. 2 (11) (2012) 4844–4856.
[51] W.S. Choi, H.M. Yang, H.Y. Koo, H.-J. Lee, Y.B. Lee, T.S. Bae, et al., Smart microcapsules encapsulating reconfigurable carbon nanotube cores, Adv. Funct. Mater. 20 (5) (2010) 820–825.
[52] S. Deng, R. Bai, Adsorption and desorption of humic acid on aminated polyacrylonitrile fibers, J. Colloid Interface Sci. 280 (1) (2004) 36–43.
[53] A. El-Sikaily, A.E. Nemr, A. Khaled, O. Abdelwehab, Removal of toxic chromium from wastewater using green alga Ulva lactuca and its activated carbon, J. Hazard. Mater. 148 (1–2) (2007) 216–228.
[54] Y. Ho, J. Porter, G. McKay, Equilibrium isotherm studies for the sorption of divalent metal ions onto peat: copper, nickel and lead single component systems, Water Air Soil Poll. 141 (1–4) (2002) 1–33.
[55] Y.-S. Ho, Isotherms for the sorption of lead onto peat: comparison of linear and non-linear methods, Pol. J. Environ. Stud. 15 (1) (2006) 81–86.
[56] K.V. Kumar, S. Sivanesan, Prediction of optimum sorption isotherm: comparison of linear and non-linear method, J. Hazard. Mater. 126 (1) (2005) 198–201.
[57] J.H. Zhu, S.Y. Wei, H.B. Gu, S.B. Rapole, Q. Wang, Z.P. Luo, et al., One-Pot synthesis of magnetic graphene nanocomposites decorated with Core@ Double-shell nanoparticles for fast chromium removal, Environ. Sci. Technol. 46 (2) (2012) 977–985.
[58] M. Avila, T. Burks, F. Akhtar, M. Gothelid, P.C. Lansaker, M.S. Toprak, et al., Surface functionalized nanofibers for the removal of chromium(VI) from aqueous solutions, Chem. Eng. J. 245 (2014) 201–209.
[59] X.-F. Sun, C. Liu, Y. Ma, S.-G. Wang, B.-Y. Gao, X.-M. Li, Enhanced Cu(II) and Cr(VI) biosorption capacity on poly(ethylenimine) grafted aerobic granular sludge, Colloids Surf. B 82 (2) (2011) 456–462.
[60] X.-j. Hu, J.-s. Wang, Y.-g. Liu, X. Li, G.-m. Zeng, Z.-l. Bao, et al., Adsorption of chromium (VI) by ethylenediamine-modified cross-linked magnetic chitosan resin: isotherms, kinetics and thermodynamics, J. Hazard. Mater. 185 (1) (2011) 306–314.
[61] J. Wang, K. Pan, Q. He, B. Cao, Polyacrylonitrile/polypyrrole core/shell nanofiber mat for the removal of hexavalent chromium from aqueous solution, J. Hazard. Mater. 244–245 (2013) 121–129.
[62] C. Luo, Z. Tian, B. Yang, L. Zhang, S. Yan, Manganese dioxide/iron oxide/acid Oxidized multi-walled carbon nanotube magnetic nanocomposite for enhanced hexavalent chromium removal, Chem. Eng. J. 234 (2013) 256–265.
[63] L.S. Zhong, J.S. Hu, H.P. Liang, A.M. Cao, W.G. Song, L.J. Wan, Self-assembled 3D flowerlike iron oxide nanostructures and their application in water treatment, Adv. Mater. 18 (18) (2006) 2426–2431.
[64] H.B. Gu, S.B. Rapole, Y.D. Huang, D.M. Cao, Z.P. Luo, S.Y. Wei, et al., Synergistic interactions between multi-walled carbon nanotubes and toxic hexavalent chromium, J. Mater. Chem. A 1 (6) (2013) 2011–2021.
[65] Y. Cao, Y. Li, H. Yu, F. Peng, H. Wang, Aerobic oxidation of α-pinene catalyzed by carbon nanotubes, Catal. Sci. Tech. 5 (8) (2015) 3935–3944.
[66] Y. Cao, H. Yu, F. Peng, H. Wang, Selective allylic oxidation of cyclohexene catalyzed by nitrogen-doped carbon nanotubes, ACS Catal. 4 (2014) 1617–1625.
[67] H. Yu, F. Peng, J. Tan, X.W. Hu, H.J. Wang, J.A. Yang, et al., Selective catalysis of the aerobic oxidation of cyclohexane in the liquid phase by carbon nanotubes, Angew. Chem. Int. Ed. 50 (17) (2011) 3978–3982.
[68] G. Zhong, H. Wang, H. Yu, F. Peng, Nitrogen doped carbon nanotubes with encapsulated ferric carbide as excellent electrocatalyst for oxygen reduction reaction in acid and alkaline media, J. Power Sources 286 (0) (2015) 495–503.
[69] X.S. Zhou, F. Peng, H.J. Wang, H. Yu, J.A. Yang, Preparation of B, N-codoped nanotube arrays and their enhanced visible light photoelectrochemical performances, Electrochem. Commun. 13 (2) (2011) 121–124.
[70] X.S. Zhou, F. Peng, H.J. Wang, H. Yu, J.A. Yang, Effect of nitrogen-doping temperature on the structure and photocatalytic activity of the B,N-doped TiO_2, J. Solid State Chem. 184 (1) (2011) 134–140.
[71] R.P. Iczkowski, J.L. Margrave, Electronegat. J. Am. Chem. Soc. 83 (17) (1961) 3547–3551.
[72] C.L. Chen, J. Zhang, B.S. Zhang, C.L. Yu, F. Peng, D.S. Su, Revealing the enhanced catalytic activity of nitrogen-doped carbon nanotubes for oxidative dehydrogenation of propane, Chem. Commun. 49 (74) (2013) 8151–8153.
[73] J. Hu, C. Chen, X. Zhu, X. Wang, Removal of chromium from aqueous solution by using oxidized multiwalled carbon nanotubes, J. Hazard. Mater. 162 (2) (2009) 1542–1550.